Molecular Level Processes and Nanostructure Evolution During the Formation of the Cubic Mesoporous Material KIT-6

Sharon Ruthstein,[†] Judith Schmidt,[‡] Ellina Kesselman,[‡] Ronit Popovitz-Biro,[§] Liora Omer,[†,‡] Veronica Frydman,[§] Yeshayahu Talmon,[‡] and Daniella Goldfarb*[,†]

Department of Chemical Physics and the Chemical Research Support Unit, The Weizmann Institute of Science, Rehovot 76100, Israel, and Department of Chemical Engineering, Technion - Israel Institute of Technology, Haifa 32000, Israel

Received September 7, 2007. Revised Manuscript Received December 25, 2008

This study focuses on the formation mechanism of the bicontinuous cubic $Ia\bar{3}d$ mesoporous material KIT-6, both on the molecular and on the mesoscopic levels. KIT-6 is synthesized with Pluronic P123 ($PEO_{20}PPO_{70}PEO_{20}$), low acid concentration, and *n*-butanol at 40 °C. Through in situ EPR measurements on a series of spin-labeled Pluronic molecules introduced at minute quantities into the reaction mixture, changes in the hydrophobicity and the mobility of the polymer chains during the reaction were observed. In addition, to learn more on the functionality of the butanol in this synthesis, freeze-quench electron spin–echo envelope modulation (ESEEM) measurements on reaction mixtures in D_2O and in butanol-d_{10} were preformed. The above experiments gave information on variations in the butanol location and content in the micellar structures during the formation of KIT-6. The evolution of the solution nanostructures was determined by cryo-TEM. Five main stages were resolved: the first two occurred during the first 140 min of the reaction, where condensation of the silica oligomers takes place at the micellar/water interface; this induces depletion of water and butanol molecules from the core−corona interface and reduces the mobility of the ends of the Pluronic chains located at the corona−water interface. This in turn leads to a transition from spheroidal micelles to threadlike micelles and to their aggregation toward the end of the second stage. During the third stage, precipitation (140–160 min), reorganization in the micellar structure, and a change in the relative sizes of core and corona take place. The fourth stage, that ends around 6 h, involves the formation of a hexagonal phase, through accelerated condensation of silica oligomers in the corona, accompanied by extensive depletion of water and butanol molecules. The presence of butanol in the micelle corona is essential in the last stage, 6–24 h, where the cubic phase is formed. We show that the addition of butanol to the reaction mixture of SBA-15 after the formation of the hexagonal phase leads to the formation of the cubic phase.

Introduction

Mesoporous materials with large pore diameter, in the range of 2–30 nm, are obtained using nonionic block copolymer surfactants, such as poly(ethylene oxide)−poly(propylene oxide)−poly(ethylene oxide) (Pluronics, PEO_xPPO_y PEO_x).[1] The two-dimensional (2D)-hexagonal SBA-15 was the first material that was synthesized with Pluronic.[2] It has attracted considerable attention because of its high structure regularity, thick inorganic walls, and excellent thermal and hydrothermal stability, its low-cost and nontoxic template, and because the simple and reproducible synthesis. In addition, one of the interesting properties of SBA-15 is the coexistence of meso- and micropores.[3] The source of the microporosity has been ascribed to PEO chains that are trapped in the silica network during the synthesis and are removed by calcination, leaving open micropores.[3–5]

Mesoporous materials consisting of interconnected large cage-type pores (>5 nm), organized in a three-dimensional network, are expected to be superior to hexagonal structures with one-dimensional channels for applications involving selectively tuned diffusion, immobilization of large molecules, or host–guest interactions in nanostructured materials.[6,7] However, mesoporous materials with cubic symmetry are usually more difficult to prepare than the 2D hexagonal counterparts, and they can be obtained only in a narrow range of synthesis mixture compositions.[1,6,8] Recent reports indicate that bicontinuous body-centered ($Ia\bar{3}d$) cubic mesostructured silica with large pores can be obtained using additives such

[†] Department of Chemical Physics, The Weizmann Institute of Science.
[‡] Technion - Israel Institute of Technology.
[§] Chemical Research Support Unit, The Weizmann Institute of Science.

(1) Zhao, D.; Huo, Q.; Feng, J.; Chmelka, B. F.; Stucky, G. D. *J. Am. Chem. Soc.* **1998**, *120*, 6024.
(2) Zhao, D.; Feng, J.; Huo, Q.; Melosh, N.; Fredrickson, G.; Chmelka, B.; Stucky, G. D. *Science* **1998**, *279*, 548.
(3) Ryoo, R.; Ko, C. H.; Kruk, M.; Antochshuk, V.; Jaroniec, M. *J. Phys. Chem. B* **2000**, *104*, 11465.
(4) Impéror-Celrc, M.; Davidson, P.; Davidson, A. *J. Am. Chem. Soc.* **2000**, *122*, 11925.
(5) Ruthstein, S.; Frydman, V.; Kababya, S.; Landau, M.; Goldfarb, D. *J. Phys. Chem. B.* **2003**, *107*, 107.
(6) Alfredsson, V.; Anderson, M. W. *Chem. Mater.* **1996**, *8*, 1141.
(7) Sakamoto, Y.; Kim, T-W.; Ryoo, R.; Terasaki, O. *Angew. Chem., Int. Ed.* **2004**, *43*, 5231.
(8) Voort, P. V. D.; Ravikovitch, P. I.; Jong, K. P. D.; Neimark, A. V.; Janssen, A. H.; Benjelloun, M.; Van Bavel, E.; Cool, P.; Weckhuysen, B. M.; Vansant, E. F. *Chem. Commun.* **2002**, 1010.

10.1021/cm7025619 CCC: $40.75
Published on Web 03/18/2008

as inorganic salts and anionic surfactants[9] with or without a swelling agent.[10] Recently, Ryoo and co-workers[11–13] reported a simple synthesis route to high-quality cubic $Ia\bar{3}d$ silica, using Pluronic P123 and *n*-butanol at low acid conditions. The advantage of this synthesis is its high reproducibility and the relatively large range of compositions that produce the ordered cubic phase. For a number of synthesis procedures of the bicontinuous cubic phase, it was reported that variation in the relative amounts of additives can lead to a transition from 2D hexagonal to cubic material.[9,10,13]

Mesoporous materials are interesting also because of their fascinating formation mechanism. In principle, the formation mechanism can be viewed at three length scales: (i) the molecular one, which involves the interaction between the organic and the inorganic precursors and the silica polymerization process; (ii) the mesoscopic scale, which involves the development of the micellar structure and the onset of the long-range order; and finally (iii) the macroscale which is related to the shape/morphology of the final product. It is clear that the processes at the molecular level are the driving force for the mesoscale structure, but the question is how the two scales are correlated.

Many studies that have focused on the formation mechanism of various types of templated mesoporous materials have been summarized in a number of reviews.[14–17] For dilute systems, where the surfactant concentration is low, such that liquid crystalline phases are not preformed, it is generally accepted that the formation of mesoporous materials occurs in two steps. The initial stage involves one of the following processes: (i) preferable adsorption of silicate ions at the micellar interface, driven either by charge matching or hydrogen bonding,[18,19] or (ii) the silicate oligomers not adsorbing at the micellar interface but instead forming siliceous prepolymers that bind surfactant molecules in a cooperative manner, resulting in the formation of new silica−surfactant hybrid micellar aggregates.[20] Most of the experimental results are, however, more consistent with (i) than (ii).[21–24] The next step involves also two possibilities: (i) Silicate adsorption leads to rearrangement of the original micellar morphology, mainly lengthening the micelles, followed by condensation of the silicate-covered micelles into ordered or disordered collapsed phases. (this is often referred to as cooperative self-assembly mechanism [21]) (ii) Alternatively, silicate adsorption does not change the morphology of the micelles but rather reduces the intermicellar repulsion. This causes aggregation into larger particles and precipitation of a disordered phase, which then may rearrange to form an ordered phase.[25,26]

To account for the different phases formed, the surfactant packing parameter, $g = v/a_0 l$,[27,28] has been used to describe the surfactant organization in the self-assembly arrays and to predict the resulting mesostructures.[1,29] v is the chain volume of the surfactant, a_0 is the effective hydrophobic/hydrophilic interfacial area, and l is the kinetic surfactant chain length.[27,28] The larger g, the lower the aggregate curvature. g can be controlled by changing a_0 through charge matching between the surfactant headgroup and the forming silanoate in the case of charged surfactants. For nonionic surfactants, like Pluronics, a_0 is controlled via the hydration of the PEO groups, which comprise the corona, that serve as effective headgroup.[30] Another way to change g is through the organic chain packing. The charge-matching is mainly controlled by the pH, the cosurfactant concentration, and the counteranion, whereas the organic packing is influenced by temperature and organic additives.[31]

Most of the mechanistic studies reported so far have focused on one length scale, and only a few attempts to correlate different length scales using different techniques have been reported. Examples are the application of in situ ^{1}H NMR (nuclear magnetic resonance) SAXS (small angle X-ray scattering), and TEM (transmission electron microscopy) in the study of the formation mechanism of SBA-15 by Flodström et al.[26] In an earlier study we have combined in situ continuous wave (CW) electron paramagnetic resonance (EPR) and freeze-quench electron spin–echo envelope modulation (ESEEM) spectroscopy of spin probes with cryo-TEM (cryogenic-temperature TEM) in the study of the formation mechanism of SBA-15.[32] Such EPR techniques had already been employed in the investigation of the formation of MCM-41.[33–36] In these experiments molecular level information on the evolution of the tumbling rate of

(9) Chen, D.; Li, Z.; Yu, C.; Shi, Y.; Zhang, Z.; Tu, B.; Zhao, D. *Chem. Mater.* **2005**, *17*, 3228.
(10) Chen, D.; Li, Z.; Wan, Y.; Tu, X.; Shi, Y.; Chen, Z.; Shen, W.; Yu, C.; Tu, B.; Zhao, D. *J. Mater. Chem.* **2006**, *16*, 1511.
(11) Kleitz, F.; Choi, S. H.; Ryoo, R. *Chem. Commun.* **2003**, 2136.
(12) Kleitz, F.; Liu, D.; Anilkumar, G. M.; Park, I.-S.; Solovyov, L. A.; Shmakov, A. N.; Ryoo, R. *J. Phys. Chem. B* **2003**, *107*, 14296.
(13) Kim, T.-W.; Kleitz, F.; Paul, B.; Ryoo, R. *J. Am. Chem. Soc.* **2005**, *127*, 7601.
(14) Ying, J. Y.; Mehnert, C. P.; Wong, M. S. *Angew. Chem., Int. Ed.* **1999**, *38*, 56.
(15) Wan, Y.; Zhao, D. Y. *Chem. Rev.* **2007**, *107*, 2821.
(16) Epping, J. D.; Chmelka, B. F. *Curr. Opin. Colloid Interface Sci.* **2006**, *11*, 81.
(17) Edler, K. J. *Aust. J. Chem.* **2005**, *58*, 627.
(18) Huo, Q.; Margolese, D. I.; Ciesla, U.; Feng, P.; Gier, T. E.; Sieger, P.; Leon, R.; Petroff, P.; Schüth, F.; Stucky, G. D. *Nature* **1994**, *368*, 317.
(19) Tanev, P. T.; Pinnavia, T. J. *Science* **1995**, *267*, 865.
(20) Frasch, J.; Lebeau, B.; Soulard, M.; Patarin, J.; Zana, R. *Langmuir* **2000**, *16*, 9049.
(21) Firouzi, A.; Kumer, D.; Bull, L. M.; Besier, T.; Sieger, P.; Huo, Q.; Walker, S. A.; Zasadzinski, A.; Glinka, C.; Nicol, J.; Margolese, D.; Stucky, G. D.; Chmelka, B. F. *Science* **1995**, *267*, 1138.
(22) Holmes, S. M.; Zholobenko, V. L.; Thursfield, A.; Plaisted, R. J.; Cundy, C. S.; Dwyer, J. *J. Chem. Soc., Farady Trans.* **1998**, *94*, 2025.
(23) Melosh, N. A.; Lipic, P.; Bates, F. S.; Wudl, F.; Stucky, G. D.; Fredrickson, G. H.; Chmelka, B. F. *Macromolecules* **1999**, *32*, 4332.
(24) Ruthstein, S.; Frydman, V.; Goldfarb, D. *J. Phys. Chem. B* **2004**, *108*, 9016.
(25) Flodström, K.; Wennerström, H.; Teixeira, C. V.; Amenitsch, H.; Lindén, M.; Alfredsson, V. *Langmuir* **2004**, *20*, 10311.
(26) Flodström, K.; Wennerström, H.; Alfredsson, V. *Langmuir* **2004**, *20*, 680.
(27) Israelchvili, J. N.; Mitchell, D. J.; Ninharn, B. *J. Chem. Soc., Faraday Trans. 2* **1976**, *72*, 1525.
(28) Israelchvili, J. N. *Intermolecular and Surface Forces*, 2nd ed.; Academic: London, 1990.
(29) Ciesla, U.; Schüth, F. *Microporous Mesoporous Mater.* **1999**, *27*, 131.
(30) Kipkemboi, P.; Fogden, A.; Alfredsson, V.; Flodström, K. *Langmuir* **2001**, *17*, 5398.
(31) Lin, H.-P.; Mou, C.-Y. *Acc. Chem. Res.* **2002**, *35*, 927.
(32) Ruthstein, S.; Schmidt, J.; Kesselman, E.; Talmon, Y.; Goldfarb, D. *J. Am. Chem. Soc.* **2006**, *128*, 3367.
(33) Zhang, J.; Luz, Z.; Goldfarb, D. *J. Phys. Chem. B* **1997**, *101*, 7087.
(34) Zhang, J.; Luz, Z.; Zimmermann, H.; Goldfarb, D. *J. Phys. Chem. B* **2000**, *104*, 279.
(35) Zhang, J.; Carl, P. J.; Zimmermann, H.; Goldfarb, D. *J. Phys. Chem. B* **2002**, *106*, 5382.

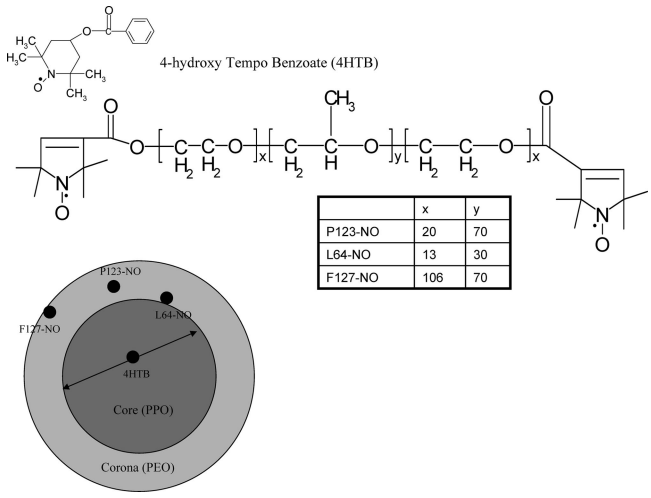

	x	y
P123-NO	20	70
L64-NO	13	30
F127-NO	106	70

Figure 1. Spin-probes used in this study and their schematic position within the P123 micelles.

the organic molecules and the polarity and water content of their close environment during the reaction was obtained. The development of the microstructures during the reaction was studied by cryo-TEM. In cryo-TEM the supramolecular structures in solution are observed by vitrifying a thin layer of a solution without staining or drying the sample, which may change the properties of the intermediates. On the basis of these studies, we suggested a model for the formation of SBA-15.[5,24,32]

While a number of studies focused on the formation mechanism of SBA-15[5,24,26,32] less work has been done on the formation of cubic materials formed with Pluronics. Here we explore the formation mechanism of the cubic material, KIT-6, through in situ CW EPR and freeze-quench ESEEM measurements using selected Pluronic spin-labels, and cryo-TEM and freeze fracture replication (FFR) experiments, to study the nanostructures which formed during the reaction, before and after precipitation. On the basis of the EPR and TEM results we present a model for the formation of KIT-6, explain the role of the butanol, and compare it with that of SBA-15 and with other reported mechanisms for cubic phases. Moreover, the results obtained lead to an alternative synthesis procedure.

Experimental Section

Synthesis. The reagents we used for the synthesis were Pluronic P123 ($EO_{20}PO_{70}EO_{20}$, M_{av} = 5800), a gift from BASF Corp. (U.S.A.), tetra-ethoxy-orthosilane (TEOS, $(CH_3CH_2O)_4Si$ (Aldrich)), hydrochloric acid (HCl 32% Frutarom), butanol (99.7% Aldrich), and butanol-d_{10} (98%, Cambridge Isotope Laboratories, Inc.). The spin-probes employed in this study (Figure 1) were 4-hydroxy-tempo-benzoate (Aldrich), and Pluronic spin-probes, which were synthesized as described in the literature.[37] The Pluronic spin-probes are Pluronic molecules with nitroxides attached to the end of the PEO blocks.[24]

KIT-6 was synthesized according to the procedure reported by Kim et al.,[13] except for the addition of the spin-probe. A typical KIT-6 synthesis was as follows: to a 36 mL aqueous solution containing 1.0 g of P123 (0.172 mmol) was added 20 μmol of spin-probe at 40 °C, and the mixture was stirred for several minutes until all the spin-probe dissolved. Then, 2.1 mL of 32% HCl (21.4 mmol) and 1.25 mL of BuOH (13.8 mmol) were added, and the mixture was stirred for 1 h, followed by the addition of 2.3 mL (10 mmol) of TEOS. The resulting mixture was left under stirring for 24 h at 40 °C. Then, half of the gel solution was filtered and dried at 100 °C for 24 h. The other half of the gel solution was subjected to a hydrothermal treatment. It was transferred into a Teflon bottle and heated at 100 °C for 24 h without stirring. After cooling to room temperature, the solid product was recovered by filtering and dried at 100 °C for 24 h. The molar composition of the synthesis gel was TEOS, 1.7×10^{-2}; P123, 2.1; HCl, 200; H_2O, 1.38; BuOH, 2×10^{-3} spin-probe.

Spectroscopic Measurements. EPR spectra were recorded using a X-band Bruker Elexsys 500 spectrometer. Gel and liquid samples were measured in flat cells and solid samples in 3 mm o.d. quartz tubes. In situ EPR measurements were carried out as follows: The P123 solution was first prepared, and then HCl + BuOH were added under stirring; after 1 h TEOS was added under vigorous stirring as described above. Ten minutes later part of the mixture was quickly transferred into an EPR flat cell, which was kept in the EPR cavity until the end of the measurement at 40 °C. The solid formed during the experiment remained within the active part of the cavity throughout the measuring period. The remaining solution was left on the hot-plate outside with no stirring. SAXS of the final material showed that the cubic structure formed also without stirring. In addition, all visible effects, turbidity and precipitation, were observed at the same time, both in the flat cell and in the remaining solution.

ESEEM experiments were carried out at X-band frequencies in 3.6 mm o.d. Teflon tubes with a Bruker Elexsys E 580 spectrometer. Because ESEEM experiments must be conducted at low temperatures to slow the echo decay and to eliminate averaging of hyperfine anisotropy by motion, reaction mixtures at 40 °C were quenched by rapid freezing in iso-pentane cooled by liquid nitrogen at different reaction times. The three-pulse ESEEM sequence, $\pi/2 - \tau - \pi/2 - T - \pi/2 - \tau -$ echo , was employed with a four-step phase cycling.[38] The $\pi/2$ pulse length was 20 ns, and τ was set to 224 ns to optimize ^{2}H modulation; the field was set to maximize echo intensity ($M_I = 0$ component). The modulation depth was taken as $k = a/(a + b)$, where $a + b$ is the interpolated echo intensity between the first and the second maxima and b is the echo intensity at the first minimum.[24]

SAXS measurements on dried products were carried out on a homemade SAXS diffractometer, equipped with a Franks mirror and one-dimensional position-sensitive detector, using Cu Kα radiation (1.54 Å) with a Ni filter.[39]

The surface area and pore size distribution were obtained from nitrogen adsorption–desorption isotherms measured at 77 K with a NOVA-1000 instrument (Quantachrome, version 7.11) using conventional Braunauer−Emmett−Teller (BET) and BJH methods. The sample was outgassed for 3 h under vacuum at 200 °C prior to analysis.

Data Treatment and Spectral Simulation. EPR spectra of the final material were simulated using the NLSL program developed by Budil et al.,[40,41] where the dynamic parameters characterizing

(36) Galarneau, A.; Di Renzo, F.; Fajula, F.; Mollo, L.; Fubini, B.; Ottaviani, M. F. *J. Colloid Interface Sci.* **1998**, *201*, 105.
(37) Caragheorgheopol, A.; Caldararu, H.; Dragutan, I.; Joela, H.; Brown, W. *Langmuir* **1997**, *13*, 6912.
(38) Fauth, J. M.; Schweiger, A.; Braunschweiler, L.; Forrer, J.; Ernst, R. R. *J. Magn. Reson.* **1986**, *66*, 74.
(39) Cheethman, J. J.; Wachtel, E.; Bach, D.; Epand, R. M. *Biochemistry* **1989**, *28*, 8928.
(40) Budil, D. E.; Lee, S.; Saxena, S.; Freed, J. H. *J. Magn. Reson. A* **1996**, *120*, 155.

the molecular motion are obtained by a nonlinear least-squares fit of the experimental spectrum to model calculations based on the stochastic Liouville equation. We used a Brownian diffusion model and an axially symmetric rotational diffusion tensor, thus defining two rate constants, $R_{\|}$ and $R_{\perp}$. The simulations require the principal components of the **g** and **A** tensors. The principal **g** values of Pluronic spin-probes were assumed to be similar to the **g** values of L62-NO, determined previously by recording a spectrum at W band,[5] yielding $g_{xx} = 2.0069$, $g_{yy} = 2.0052$, and $g_{zz} = 2.0000$. The values $A_{xx} = A_{yy} = 0.58$ mT and $A_{zz} = 3.52$ mT were determined by fitting the rigid limit spectrum of KIT-6 with F127-NO. We used the same hyperfine coupling for the two species observed experimentally, because the changes in the local polarity is small compared to the inhomogeneous line width, and in the final material the differences between the two types are governed by the rotational diffusion rates.

The high-field component of the EPR spectra recorded during the reaction, was simulated using a superposition of two Lorentzian lines. From this simulation a_N, the line-width and the relative amount of each species were determined. The isotropic rotational correlation time, τ_c (in seconds) for a spectrum characterized by one species has been calculated according to the formula:[42]

$$\tau_c = (6.51 \times 10^{-10})\Delta H(0)\{[h(0)/h(-1)]^{1/2} + [h(0)/h(1)]^{1/2} - 2\}$$

where $\Delta H(0)$ is the peak-to-peak line width in Gauss of the $M_I = 0$ component, and $h(-1)$, $h(0)$, and $h(1)$ are the peak to peak heights of the $M = -1$, 0, and $+1$ lines, respectively. For a spectrum with two species, τ_c was obtained through simulations using the program Garlic of the Easyspin software package,[43] with g = (2.0069, 2.0052, 2.0000), and a_N, line-width, and the relative amount of each species obtained from the deconvolution of the high-field component as described above were used as starting values.

FT of the three pulse ESEEM traces was carried out as follows: The traces were phased and normalized to 1, after which a polynomial baseline correction was preformed, followed by apodization with an exponential window and zero filling to 512 points. Finally, FT was performed, and magnitude spectra were calculated using cross-term averaging.[44] All these manipulations were carried out with Matlab (The Mathworks, Inc.).

Microscopy Measurements. Vitrified specimens for cryo-TEM were prepared in a controlled environment vitrification system (CEVS). [45] All solutions were quenched from 40 °C and 100% relative humidity by plunging into liquid ethane at its freezing point. Specimens were examined in a FEI Tecnai T12 microscope, operated at 120 kV, using a Gatan Instruments 626 DH cryo-holder system. All specimens were observed in the microscope approximately at −170 °C. Images were recorded digitally in the minimal electron dose mode by a Gatan High Resolution US1000 cooled-CCD camera with the DigitalMicrograph software package.

Freeze-fracture-replication (FFR) was performed with a BAF-060 system (BalTec AG, Liechtenstein). A small drop of the sample was placed on an electron microscopy copper grid and sandwiched between two gold planchettes. The sandwich was plunged into liquid ethane at its freezing point, transferred into liquid nitrogen, and inserted into a sample fracture block, precooled by liquid nitrogen. The block was inserted into the BAF-system vacuum chamber, maintained at −160 to −170 °C, and split open to fracture the frozen sample drop. The fracture surfaces were first etched at −110 °C for 30 s and then shadowed at a 15 ° angle with a 2 nm layer of platinum carbon, followed by backing with a 20 nm thick carbon layer. The replicas were retrieved from the thawed samples, cleaned first in 6% hydrofluoric acid (prepared from HF 38–40%, Merck) and then in double-distilled water, mounted on TEM grids, and examined in the FEI T12 TEM (see above) at room temperature.

TEM samples of the final KIT-6 product were prepared by dispersing the powder in 1:1 EtOH/water solution, followed by 30 min of sonication. Then drops of the dispersion were deposited on a carbon/collodion-coated 300 mesh copper grid and were air-dried. The specimens were examined by Philips CM120 or FEI T12 transmission electron microscope operated at 120 kV. Digital images were recorded by a Gatan US1000 CCD camera, and fast Fourier transforms (FFT) of the images were calculated by DigitalMicrograph software.

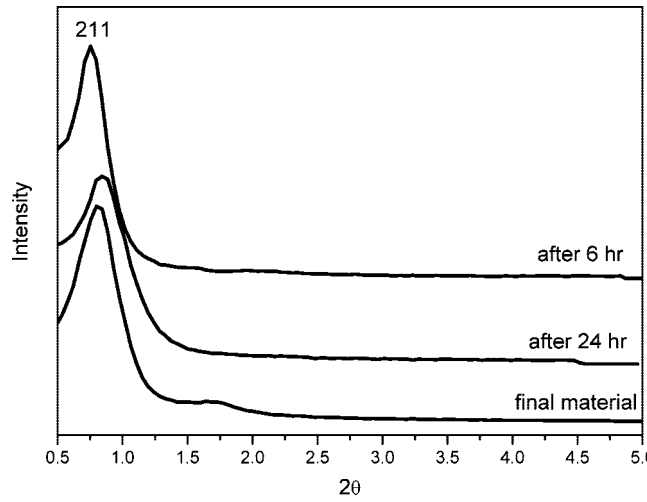

Figure 2. SAXS powder diffraction patterns of as-synthesized KIT-6, after 6 h and 24 h, and of the final material, after the hydrothermal treatment.

Results

Characterization of KIT-6. The synthesis of KIT-6 is usually carried out in two stages. The first takes place at 40 °C for 24 h, while stirring the reaction mixture. The second stage involves thermal treatment, where the aged gel, placed in a Teflon bottle, is heated to 100 °C for 24 h. During the first stage the solution becomes turbid around 120 min, and precipitation occurs at 140–160 min after the addition of TEOS. When stopping the reaction 6 h after adding TEOS, the SAXS pattern of the dry solid is characterized by a single diffraction peak, corresponding to a d-spacing of 117 Å (Figure 2). After 24 h of reaction at 40 °C, the single SAXS diffraction corresponds to $d = 105$ Å, and the diffraction peak is broader than at 6 h, as shown in Figure 2. After the hydrothermal stage, a second peak appears and the diffraction pattern suggests a cubic structure, with $d_{211} = 98$ Å. The broad peaks are attributed to small domains with different orientations as was explained earlier.[56] The cubic structure was confirmed by TEM images of solids obtained before and after the hydrothermal stage, presented in Figure 3. The Fourier transform (FT) shows the (220), (112), and (004)

(41) Schnider, D. J.; Freed, J. H. In *Biological Magnetic Resonance. Spin Labeling*; Berliner, L. J., Reuben, J., Eds.; Plenum: New York, 1989; Vol *8*, Chapter 1.
(42) Norodio, P. L. In *Spin Labeling, Theory and Apllications*; Berliner, L. J., Ed.; Academic Press, Inc.: London, 1976; Chapter 2.
(43) Stoll, S.; Schwiger, A. *J. Magn. Reson.* **2006**, *178*, 42.
(44) Van Doorslaer, S.; Sierra, G. A.; Schweiger, A. *J. Magn. Reson.* **1999**, *136*, 152.
(45) Talmon, Y. In *Modern Characterization Methods of Surfactants Systems*; Binks, B. P., Ed.; Marcel Dekker: New York, 1999; p 147.

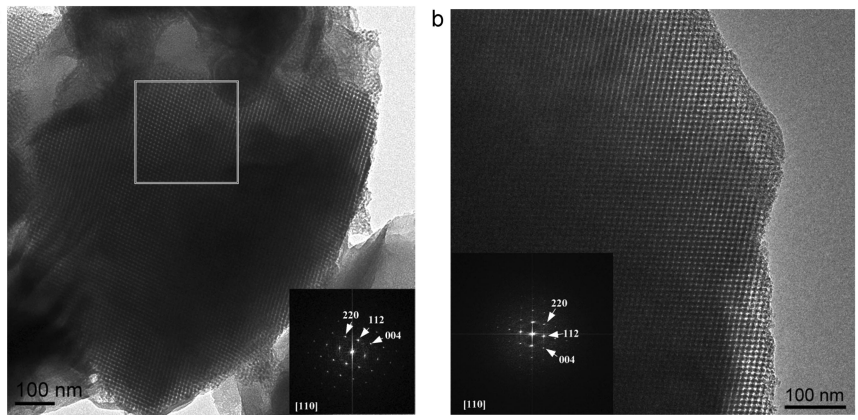

Figure 3. TEM images of (a) dry KIT-6, before hydrothermal treatment, and of (b) calcined KIT-6, after hydrothermal treatment. The area within the large box and in (b) is typical of [110] direction. The insets show the FFT with the assigned reflections.

reflections typical of the $Ia\bar{3}d$ cubic phase. The d-values of the as-synthesized material before and after hydrothermal treatment yield $a = 24.8$ and 23.6 nm, respectively, in agreement with earlier reports.[11,13] These results show that the cubic structure is formed prior to the hydrothermal stage, although it is still not well ordered, and therefore its SAXS lacks the second peak. Nitrogen adsorption isotherm measured on a calcined material after hydrothermal treatment gave an average pore size of 87.4 Å and surface area of 598.4 m^2/g, in agreement with Kleitz et al.[11] The addition of the spin probes to the reaction mixture did not alter the final material.

The effect of the hydrothermal stage on the final material was studied by EPR using different spin-probes, which are located at different positions in the P123 micelles, as indicated in Figure 1. The micelles have a hydrophobic core, consisting principally of the PPO block, and a hydrophilic corona formed by the PEO segments.[46] 4HTB (see Figure 1) is located at the core of the micelle because of its hydrophobic nature, and the location of the spin-labels of the Pluronic spin-probes in the micelle's corona depends on their PEO chain length. L64-NO has the shortest PEO length and therefore is located at the core−corona interface region, P123-NO is located in the micelle's corona, and F127-NO, with the longest chain, is situated at the corona−water interface region. The positions of the spin-labels in the P123 micelle were determined previously by their isotropic hyperfine coupling (a_N) and by $k(^2H)$ values from ESEEM measurements of micelle solutions in D_2O.[5] The depth of the ^2H modulation depth ($k(^2H)$) gives a qualitative measure to how far the spin-label is from the corona−water interface.

The spectra of the spin-probes in the dry solid before and after the hydrothermal treatment are shown in Figure 4. The spectrum of 4HTB before the hydrothermal treatment is characterized by a single mobile species. After the hydrothermal treatment the EPR signal has disappeared due to transformation to a diamagnetic hydroxylamine in acidic solution.[47] The spectra of L64-NO and P123-NO in the dry solid obtained before hydrothermal treatment are typical of

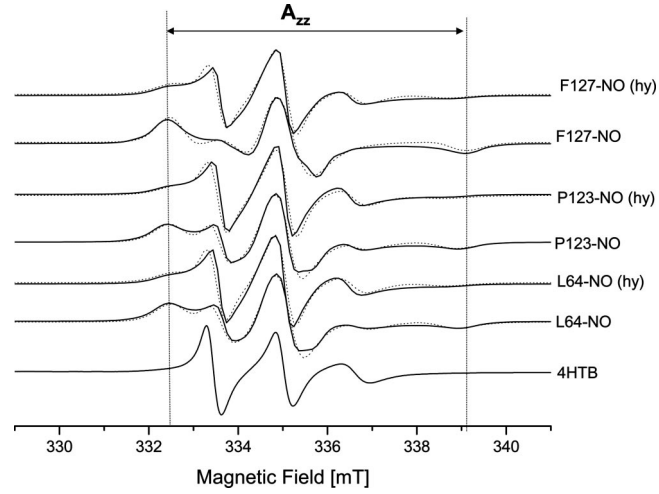

Figure 4. Room temperature CW EPR spectra of the dry solid material prepared with 4HTB, before hydrothermal treatment, and of L64-NO, P123-NO, and F127-NO before and after hydrothermal treatment (indicated in the figure as hy). The dotted lines are simulated spectra. The dashed vertical lines mark A_{zz} features of the immobile species (modulation amplitude = 1.0 G, spectrometer frequency 9.42 GHz).

a superposition of two species, one highly mobile and the other immobilized, whereas the spectrum of F127-NO shows only one rigid species with $A_{zz} = 3.35$ mT. After the hydrothermal treatment the relative amount of the immobile species of L64-NO and P123-NO decreased and a mobile species appeared for F127-NO. The relative amounts of the two species in these samples were determined using NLSL simulations, presented by dotted traces in Figure 4, and the best fit parameters are listed in Table 1. The amount of the mobile species after a hydrothermal treatment increased for all Pluronic spin-probes.

As observed here and also earlier for SBA-15,[24] the ends of the spin-probes, depending on their PEO length, are partitioned between micropores in the silica network (immobile) and the mesopores (mobile). The difference is the larger decrease the hydrothermal treatment induced on the amount of the (immobile) species trapped in the silica network for the KIT-6. This suggests 2 larger contraction of the silica layer, which increases the mesopore volume, leading to depletion of PEO chains from the silica network. This is in agreement with the increase in the mobility, $R_\perp$,

(46) Wanka, G.; Hoffman, H.; Ulbricht, W. *Macromolecules* **1994**, *27*, 4145.
(47) Rozantsev, E. G. *Free Nitroxyl Radicals*; Plenum Press: New York, 1970.

Table 1. Best-Fit Parameters Used in the Simulation Shown in Figure 4[a]

	KIT-6, (L64-NO)	KIT-6, hy[b] (L64-NO)	KIT-6, (P123-NO)	KIT-6, hy (P123-NO)	KIT-6, (F127-NO)	KIT-6, hy (F127-NO)
	immobile/mobile	immobile/mobile	immobile/mobile	immobile/mobile	immobile	immobile/mobile
$R_\perp$ 10^8 s^{-1}	0.16/1.0	0.25/1.0	0.16/1.0	0.25/1.0	0.1	0.25/1.0
$R_\parallel \times 10^8$ s^{-1}	0.032/1.6	0.032/1.6	0.032/1.6	0.032/1.6	0.002	0.032/1.6
line-width [mT]	0.3/0.5	0.3/0.5	0.3/0.5	0.3/0.5	0.5	0.3/0.5
extent of mobile species	16%	37%	14%	36%	0	30%

[a] The tilt angle, β, in all simulations is 40°; this value gave the best-fit. [b] hy corresponds to material obtained after the hydrothermal stage.

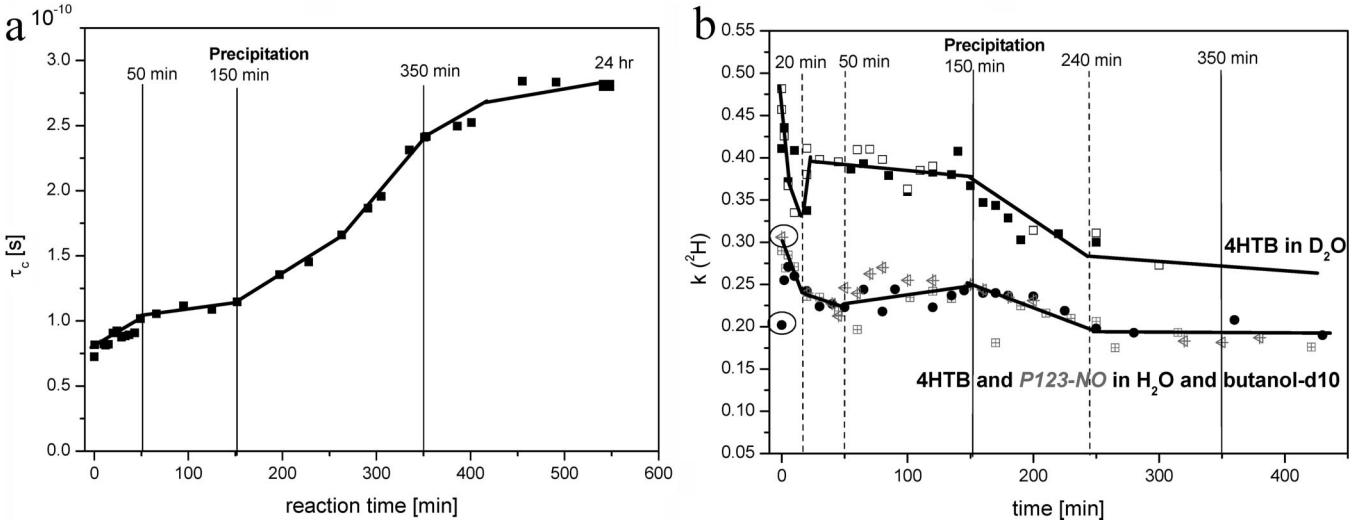

Figure 5. (a) Time evolution of τ_c of F127-NO during the formation of KIT-6 (40 °C). (b) Time evolution of $k(^2H)$ for 4HTB in a KIT-6 reaction mixture in D_2O (top trace, solid and hollow squares correspond to two different experiments), 4HTB (solid circles), and P123-NO (two different experiments, squares and triangles) in a KIT-6 reaction mixture with butanol-d_{10}. The circled data points correspond to $t = -1$ min for 4HTB and P123-NO in a P123 solution with butanol-d_{10} and HCl.

of the immobile species for all spin-probes (Table 1), due to increased volume.

EPR Measurements during the Reaction. Once the final KIT-6 material has been characterized, we proceeded to investigate the formation of KIT-6 by in situ CW EPR and ESEEM measurements. We used the same spin-probes, discussed in the previous section, which sense different regions within the P123 micelle.

F127-NO. Throughout the reaction the spectrum of F127-NO is characterized by a single highly mobile species, and the dependence of τ_c on the reaction time is shown in Figure 5a. The P123 micelle diameter is around 10 nm,[48] and its tumbling rate should be on the order of 10^{-6} s.[25] This is several orders of magnitude larger than the observed τ_c, which is on the order of 10^{-10} s (see Table 2). Thus, τ_c is determined by the local motion of the nitroxide group.[24,49] Because the label of F127-NO is located close to the corona−water interface, it is sensitive to the interaction between the micellar interface and the forming silica, and the changes in the mobility of the F127-NO are most probably associated with the condensation of the TEOS hydrolysis product. Hence, it provides information regarding the rate of formation of the silica layer. During the reaction τ_c increases, and four different stages, distinguished by their slope, can be clearly identified: (a) 0–50 min, (b) 50–150 min, (c) 150–350 min, and (d) $t > 350$ min with the largest increase in τ_c occurring between 150 and 350 min. Turbidity is observed around 120 min, and precipitation occurs around 150 min.

4HTB. The spectrum of 4HTB in the P123 micelles (indicated as $t = -5$ min) exhibits a splitting in the high field component, due to a distribution between two different environments. The addition of butanol and acid ($t = -1$ min) results in only a subtle decrease in a_N for both species (0.005–0.01 mT, see Table 2), indicating a slight increase in the hydrophobicity of the environment. During the reaction, the splitting of the high-field component persists, and Figure 6 shows the time dependence of the EPR spectrum of 4HTB at $t = 136$–180 min. The spectra of the individual components were resolved by simulations. The component with the lower ^{14}N hyperfine splitting, a_N, was termed "phob", because it is in a more hydrophobic environment, and the species with the higher a_N was termed "phil" (Figure 6). During the reaction, a_N and τ_c of both species and their relative amount vary slightly (Figure 7a,b), but at $t = 140$–160 min ($t = 0$ corresponds to the addition of TEOS), when precipitation begins, considerable variations are observed. a_N (phob) decreases considerably, R_{phob}, the relative amount of "phob", decreases from 0.77 at $t = 140$ min to 0.21 at $t = 160$ min, and τ_c (phob) increases. a_N (phil) decreases also, showing that it becomes more hydrophobic. Table 2 lists the values of a_N, τ_c, and R_{phob} at $t = 0$, 140, 160, and 240 min (obtained from simulations of the whole spectrum), and Figure 7a,b shows the time evolution of a_N and R_{phob}. At 160 min a restoration toward the initial values begins, reaching them at around 240 min.

(48) Ruthstein, S.; Potapov, A.; Raitsimring, A. M.; Goldfarb, D. *J. Phys. Chem. B* **2005**, *109*, 22843.
(49) Caragheorgheopol, A.; Caldararu, H.; Vasilescu, M.; Khan, A.; Angelescu, D.; Žiková, N.; Čejka, J. *J. Phys. Chem. B* **2004**, *108*, 7735.

Table 2. a_N, τ_c, and R_{phob} of the Various Species of the Different Spin-Probes during the KIT-6 Reaction, at t = 0 min, 140 min, 160 min, and 4 h[a]

	$t = -1$ min ($t = -5$ min)	$t = 140$ min	$t = 160$ min	$t = 4$ h	in water
		$\tau_c \times 10^{10}$ [s]			
	(phob)/(phil)	(phob)/(phil)	(phob)/(phil)	(phob)/(phil)	
4HTB	2.6/0.8	2.6/0.8	5.0/0.5	3.2/0.7	0.27 (4HT)
L64-NO	3.5/1.0	3.0/1.0	3.0/1.0	3.0/1.2	1.0
P123-NO	3.5/−	2.5/1.0	1.0/1.0	3.0/1.3	1.0
F127-NO	−/0.8	−/1.0	−/1.1	−/1.7	0.8
L62-NO in SBA-15[b]	−/2.0	2.8/2.1	2.8/2.2	2.8/2.3	1.0
		a_N [mT]			
	(phob)/(phil)	(phob)/(phil)	(phob)/(phil)	(phob)/(phil)	
4HTB	1.55 (1.55)/1.71 (1.72)	1.55/1.71	1.46/1.68	1.54/1.71	1.7 mT (4HT)
L64-NO	1.52 (1.52)/1.59 (1.59)	1.52/1.60	1.49/1.60	1.48/1.60	1.6 mT
P123-NO	1.54 (1.56)/-	1.54/1.61	1.58/1.59	1.50/1.60	1.6 mT
F127-NO	−/1.59 (1.59)	−/1.59	−/1.59	−/1.59	1.6 mT
L62-NO in SBA-15	−/1.55	1.46/1.59	1.46/1.59	1.46/1.59	1.6 mT
		R_{phob}			
4HTB	0.85 (0.85)	0.77	0.21	0.63	
L64-NO	0.94 (0.96)	0.83	0.73	0.7	
P123-NO	1.0 (1.0)	0.82	0.58	0.83	
L62-NO in SBA-15	0	0.45	0.45	0.45	

[a] Data for spin-probe in water and L62-NO in SBA-15 are given as well for comparison. [b] Synthesized with 3 wt % P123, H_3PO_4, and TMOS at 50 °C.[5]

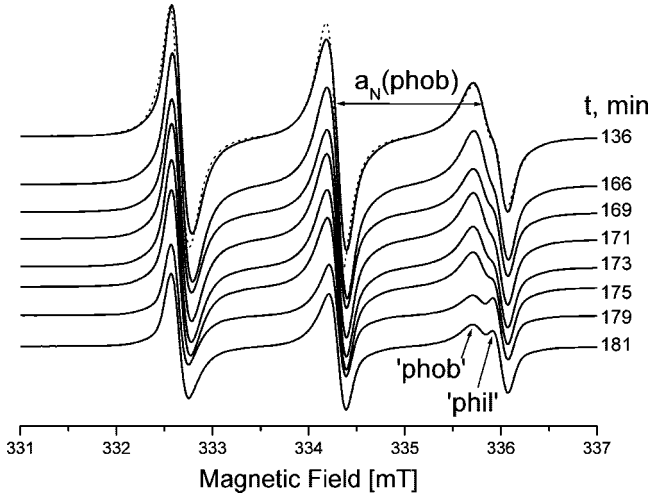

Figure 6. Time evolution of the EPR spectrum of 4HTB during the formation of KIT-6 at 40 °C. The dotted trace presents an example of a simulated spectrum with the parameters given in Table 2 (modulation amplitude = 1.0 G, spectrometer frequency 9.42 GHz).

Further insight into the formation of KIT-6, in particular at the earlier stages of the reaction, when the interaction between the silica precursors and the surfactant assemblies occurs, was obtained from ESEEM experiments. In these experiments, two types of reaction mixtures were used, one prepared in D_2O and the other in H_2O with deuterated butanol. The ^2H modulation depth ($k(^2H)$) was followed as a function of the reaction time for both types of solutions. These experiments were carried out on frozen solutions, and therefore $k(^2H)$ is a weighted average of the two species. For 4HTB, except for t = 140–160 min, "phob" constitutes the majority of the sample (~77%). The addition of BuOH + HCl to the P123 micelles in D_2O increases $k(^2H)$ from 0.09 to 0.45. This huge increase is well manifested in the ^2H peak in the FT spectra of the ESEEM traces, presented in Figure 8. The ^1H signal corresponds to protons of the polymer, the spin-probe, and BuOH.

There are two possible explanations for the increase in $k(^2H)$: (i) the destruction of the micelles and 4HTB dissolves in monomers, which, however, should be associated with a large increase in a_N, which was not observed, and (ii) solvation of butanol molecules in the micelle, which increases the solubility of the PEO and the water content of the corona, causing its swelling. The water content in the core where 4HTB is located decreases only slightly, as manifested in the subtle decrease in a_N which is affected mainly by hydrogen bonding to water molecules.[50] In contrast to a_N, $k(^2H)$ is sensitive to the presence of water molecules also at a longer distance, and therefore it increases considerably as the water content close to the core/corona interface increases.

The time evolution of $k(^2H)$ of the D_2O solution ($t \geq 0$), shown in Figure 5b, reveals four stages: (1) decrease between t = 0–20 min, (2) invariant at 20–150 min, (3) decrease at 150–240 min, at a lower rate than observed in the first 20 min, and (4) invariant at $t > 240$ min. At the precipitation time $k(^2H)$ does not exhibit a considerable change, as might have been expected because of the displacement of most of the 4HTB molecules into the hydrophilic environment, as was observed by CW EPR. However, at this time the hydrophobicity of both environments of 4HTB molecules increases, especially for the hydrophobic species, resulting in a fairly constant averaged $k(^2H)$.

The reaction mixture with butanol-d_{10} exhibited four stages as well, but with some difference in the time ranges as compared to $k(^2H)$ of the D_2O solutions. These are shown in Figure 5b. The four stages are (1) decrease between t = 0–50 min, (2) invariance at 50–150 min, (3) decrease at 150–240 min, at a lower rate than observed in the first 50 min of the reaction, and (4) invariant at $t > 240$ min.

In summary, the in situ CW EPR spectra of 4HTB revealed structural reorganization of the micelles at the precipitation time, associated with increased hydrophobicity, leading to a large change in the partition of 4HTB between its two environments. In addition, the ESEEM showed four stages where a significant depletion of water and butanol molecules

(50) Morrisett, J. D. In *Spin Labeling, Theory and Applications*; Berliner, L. J., Ed.; Academic Press, Inc.: London, 1976; Chapter 8.

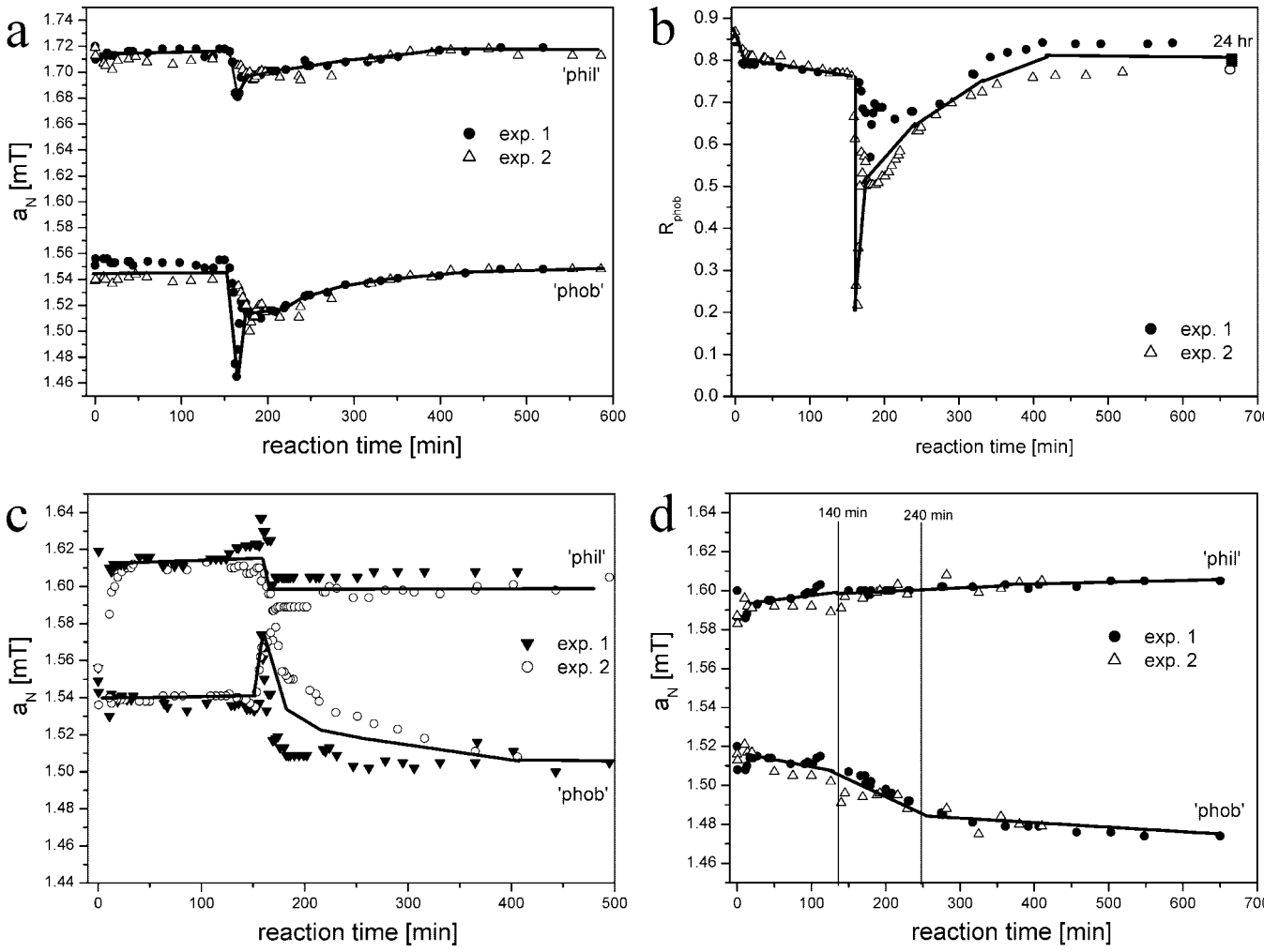

Figure 7. (a) Time evolution of a_N of the two species of 4HTB. (b) Time evolution of R_{phob} of 4HTB. (c) Time evolution of a_N of the two species of P123-NO. (d) Time evolution of a_N of the two species of L64-NO. The solid and hollow symbols indicate two different experimental sets.

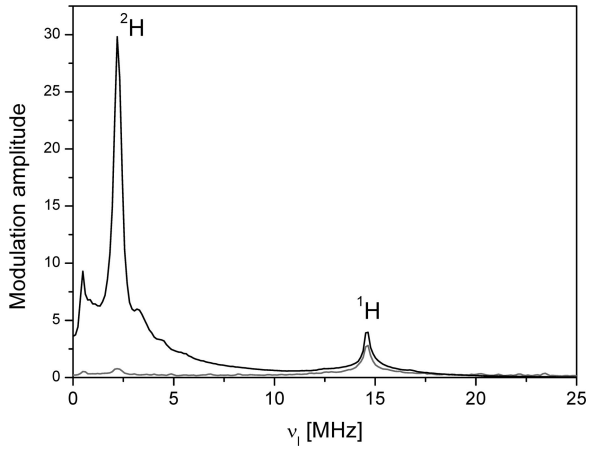

Figure 8. Magnitude FT-ESEEM spectra of 4HTB in 2.5 wt % P123 micellar solution in D_2O (gray line), before and after adding butanol with acid (dark line).

occurred after the addition of TEOS (up to approximately 50 min) and after the precipitation time, between 150 and 240 min.

P123-NO. At $t = 0$ min, the CW spectrum shows that P123-NO is located in a single environment, then, as the reaction progresses, part of it migrates to a more hydrophilic environment, first detected at $t \sim 10$ min. Similar to 4HTB, large variations occur at $t = 140$–160 min (Figure 7c). While at $t = 140$–160 min the environment of "phil" becomes more hydrophobic, that of "phob" turns more hydrophilic, opposite to 4HTB. Moreover, at this time P123-NO is partitioned rather evenly between the two environments, and τ_c (phob) decreases. At $t = 240$ min the system becomes invariant, reaching values which are slightly different than at $t = 0$ min; the environment "phob" is more hydrophobic, and also τ_c of both species decreases a little (see Table 2).

ESEEM experiments were carried out to follow the butanol content of the corona during the reaction. The time evolution of $k(^2H)$ in reaction mixture with butanol-d_{10} (gray symbols in Figure 5b) is similar to that of 4HTB, except for $t = 0$ min, where for P123-NO $k(^2H) = 0.3$ while for 4HTB it is $k(^2H) = 0.2$. This shows that the butanol prefers the corona region. However, after the addition of TEOS, at $t = 5$ min, $k(^2H) = 0.27$ for both spin-probes, indicating a displacement of butanol molecules from the corona into the core−corona interface. At $t = 5$–50 min both probes experience a reduction in $k(^2H)$, probably due to depletion of butanol from both regions. Then, up to 150 min, $k(^2H)$ stays constant for both probes, but between 150 and 240 min, a faster average depletion of butanol molecules from the core and the corona is sensed by 4HTB and P123-NO. This means that butanol

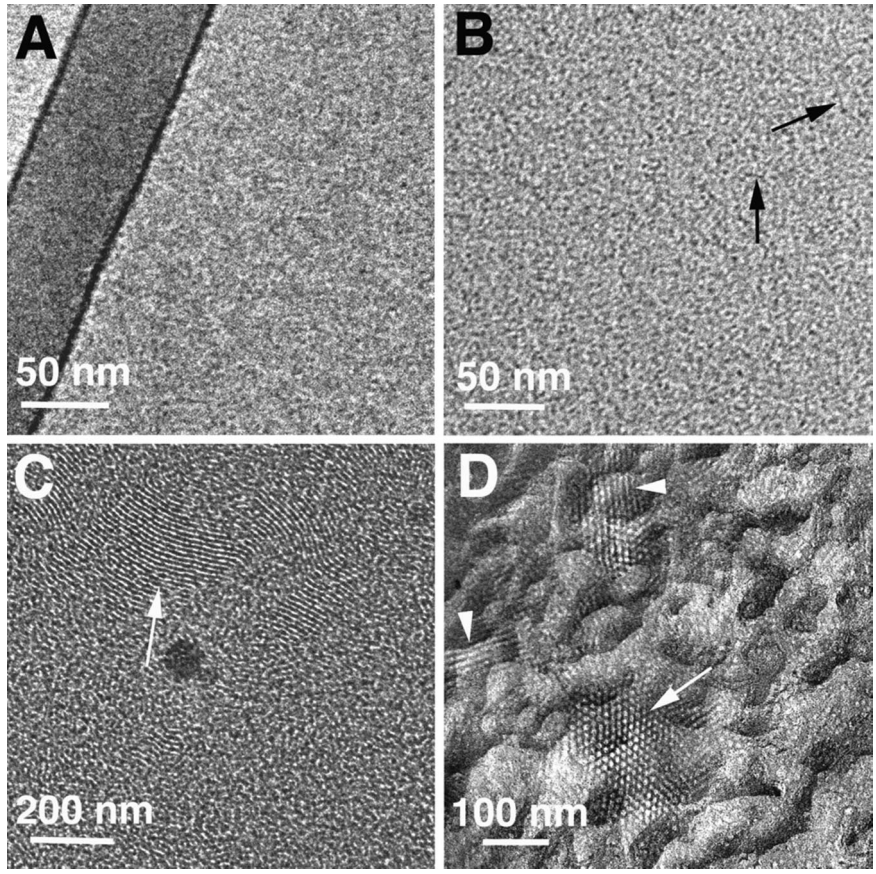

Figure 9. Cryo-TEM images following the evolution of nanostructure in the liquid phase of the KIT-6 reaction mixture. Panels A−C are direct-imaging cryo-TEM micrographs; panel D shows a freeze-fracture-replication image. Only spheroidal micelles are seen after 35 min of reaction (A). Mostly spheroidal micelles and a few TLMs (arrows) are observed after 92 min (B). Long TLMs (arrow) are seen after 132 min (C). After 238 min (D) we see a well-developed hexagonal phase: note fractures perpendicular to the long axes of the TLMs (arrow) and parallel to long axes (arrowheads).

is further displaced into the corona−water interface. From 4 h up to 24 h no change is detected for both probes, and $k(^2H) \sim 0.2$.

In summary, similar to 4HTB the reorganization of the micelles at the precipitation time was sensed by P123-NO. The butanol preferred location is in the core/corona region, and between 150 and 240 min, after the precipitation, a depletion of butanol molecules from the corona to the corona−water interface occurred.

L64-NO. The CW spectrum reveals two species at all times. While P123-NO and 4HTB are very sensitive to the reorganization that occurs at 140–160 min, L64-NO, which has a short PEO chain length, is indifferent to these changes. a_N (phil) exhibits a very mild increase during the reaction (Figure 7d) whereas a_N (phob) experiences a mild decrease during the first 140 min, which is accelerated between 140 and 240 min. During the first 240 min a continuous reduction in R_{phob} is observed, and τ_c of both species changes slightly.

The EPR spectra of the various probes after 24 h of reaction are in the fast motion region, showing that they turn immobile only after drying. This was also observed in SBA-15 showing that prior to the hydrothermal stage the silica is "soft" and not fully formed.[5]

Cryo-TEM. The nanostructures formed in the solution were explored by sampling the reaction mixture of KIT-6, held at 40 °C, as a function of time. In the synthesis of KIT-6 the reaction volume becomes visibly turbid about 120 min after the addition of TEOS, and a precipitate appears around 150 min. Thus the time limit of the direct-imaging cryo-TEM experiments was approximately 2 h.

Up to $t = 90$ min, only spheroidal micelles are observed, as can be seen in Figure 9, for $t = 35$ min. At $t = 92$ min, we observe coexistence of spheroidal micelles and individual, rather short thread-like micelles (TLMs), that later aggregate into bundles, as clearly shown at $t = 132$ min. After this time, the direct imaging cryo-TEM is not practical anymore, and we applied freeze-fracture replication (FFR). Around $t = 2.5$–3.5 h, the replicas show intermediate structure which is not clear yet, but then between 4 and 6 h, a stable hexagonal structure is present, with a spacing of 11.8 ± 0.5 nm, which is the same spacing obtained from the SAXS after 6 h of reaction.

The observation of a hexagonal phase after precipitation suggests that the BuOH may not be essential at the early stage of the reaction and may be added after the hexagonal structure has formed to generate the cubic phase. We verified this using the synthesis mixture of SBA-15 with HCl,[2] without adding butanol nor reducing the amount of HCl. In a recent study, we showed by cryo-TEM that using this procedure, the hexagonal phase is formed after approximately 20 min of reaction.[32] Thus, at $t = 25$ min (after the precipitation time, 18 min) butanol was added to the solution in a molar ratio 1:1.38 BuOH/TMOS, leaving the mixture for 24 h at 35 °C followed by hydrothermal treatment at

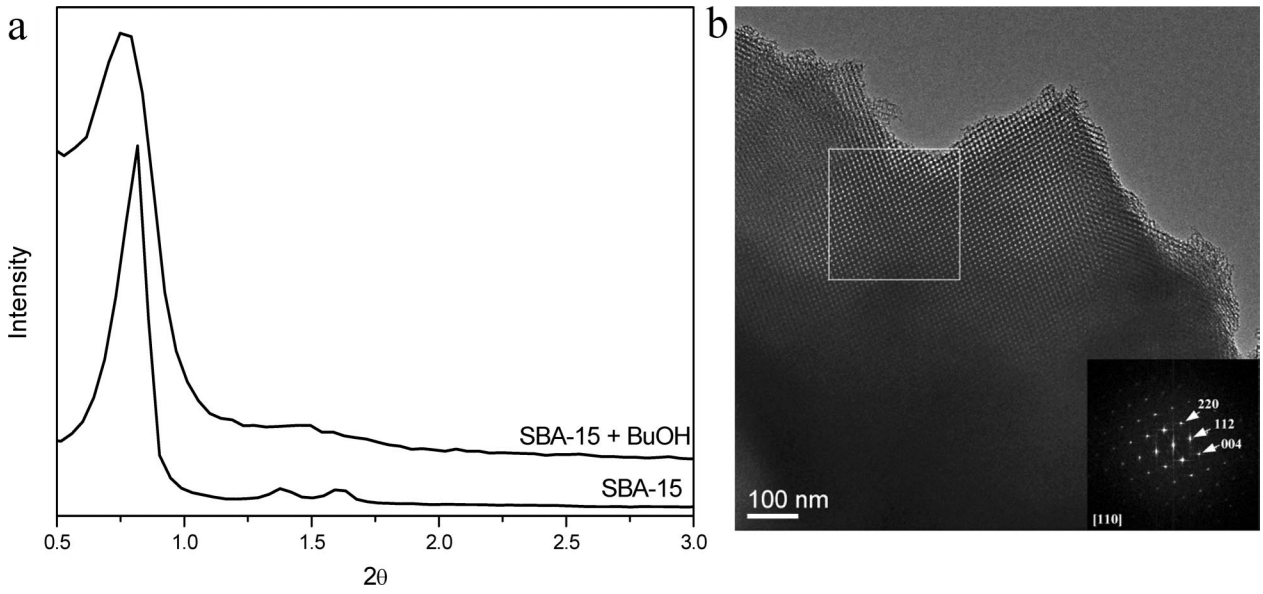

Figure 10. (a) SAXS powder patterns of SBA-15, synthesized at 35 °C with HCl, and of the solid obtained after the addition of butanol, 25 min after the addition of TMOS. (b) TEM image and the corresponding FFT of the material obtained with butanol. The area within the large box is typical of [110] direction, and the diffractions are assigned.

100 °C for 24 h. Figure 10a shows the SAXS pattern for SBA-15 and for the SBA-15 mixture with the addition of butanol. The latter is similar to that of KIT-6, and its TEM image is shown in Figure 10b. FFT of the diffractogram recorded approximately along the [110] direction shows the (220), (112), and (004) reflections which are typical for the $Ia\bar{3}d$ cubic phase. The d value yields $a = 25.2$ nm. The latter shows a diffraction pattern similar to that of the cubic phase obtained with butanol added at the beginning of the reaction (see Figure 2).

Discussion

Four aspects related to the formation of KIT-6 were explored: (i) the final material, (ii) the location of the spin-probes in the P123 micellar solution prior to the addition of TEOS, (iii) the formation mechanism at the molecular and mesoscopic level, and (iv) the role of the butanol. The discussion is structured accordingly.

Final Material. TEM images of the dry solids before and after hydrothermal treatment showed a cubic structure, and therefore the role of the hydrothermal treatment is limited to completion of the silica condensation, increasing its connectivity and yielding a material with improved order. The final material is a hybrid material with P123 (mostly the core) situated primarily within the ordered mesopores and part of the PEO chains (corona) trapped in the silica network (precursors of the micropores). The extent of the latter decreases after the hydrothermal treatment. The partitioning of the various spin-labels between mesopores and micropores correlates well with their location within the micelles, 4HTB being only in the mesopores, and the relative amount in the micropores varies as L64-NO < P123-NO < F127-NO, according to the nitroxide depth in the corona.

The hydrothermal treatment leads to large displacement of EO segments, initially trapped in the silica network, into the mesopore. This was also observed for SBA-15,[4,5,51] but to a lower extent. This suggests a larger change in the pore size for KIT-6. Indeed, Kleitz et al.[11–13] reported for KIT-6 that the pore size can increase from 4.5 to 10 nm, when increasing the temperature from 35 to 130 °C and that wall thickness decreases markedly with increasing aging. Also, in SBA-15 the pore diameter increases after the hydrothermal treatment, but by only up to 1 nm,[5] whereas for KIT-6 the pore diameter doubles after hydrothermal treatment.

Location of the Spin-Probes. Because the EPR measurements during the reaction report changes in the local environment of the spin-label, it is essential to assign their location in the P123 micelles prior to the reaction initiation, namely, in 2.5 wt % P123 aqueous solution at 40 °C. The spectra of P123-NO and F127-NO are characterized by one component, assigned to the label being in the corona and corona/water interface, respectively, on the basis of their a_N and τ_c values and earlier ESEEM experiments.[24] L64-NO and 4HTB partition between two environments, referred to as "phob" and "phil". To facilitate their assignment the spectra of the Pluronic spin-probes and 4-hydroxy-tempo (4HT) in water were recorded, and their a_N and τ_c values were determined (see Table 2). 4HT is similar to 4HTB but is water soluble. The species "phob" is located within the micelles, based on its higher τ_c and small a_N compared to the spin-probe in water. The trend found for $\delta a_N = a_N(\text{water}) - a_N(\text{phob})$, F127-NO > P123-NO > L64-NO > 4HTB, is consistent with their depth in the micelle and the extent of spin-probe trapped in silica network in the final material.

The a_N and the τ_c values of the "phil" component of L64-NO at $t = 0$ min are similar to those of the spin-probes in water (Table 2), and therefore we assign them to single chains or single chains dissolved in small oligomers of P123 in solution.[52] Similarly, we assign the "phil'" of 4HTB to spin-

(51) Galarneau, A.; Cambon, H.; Renzo, F. D.; Fajula, F. *Langmuir* **2001**, *17*, 8328.

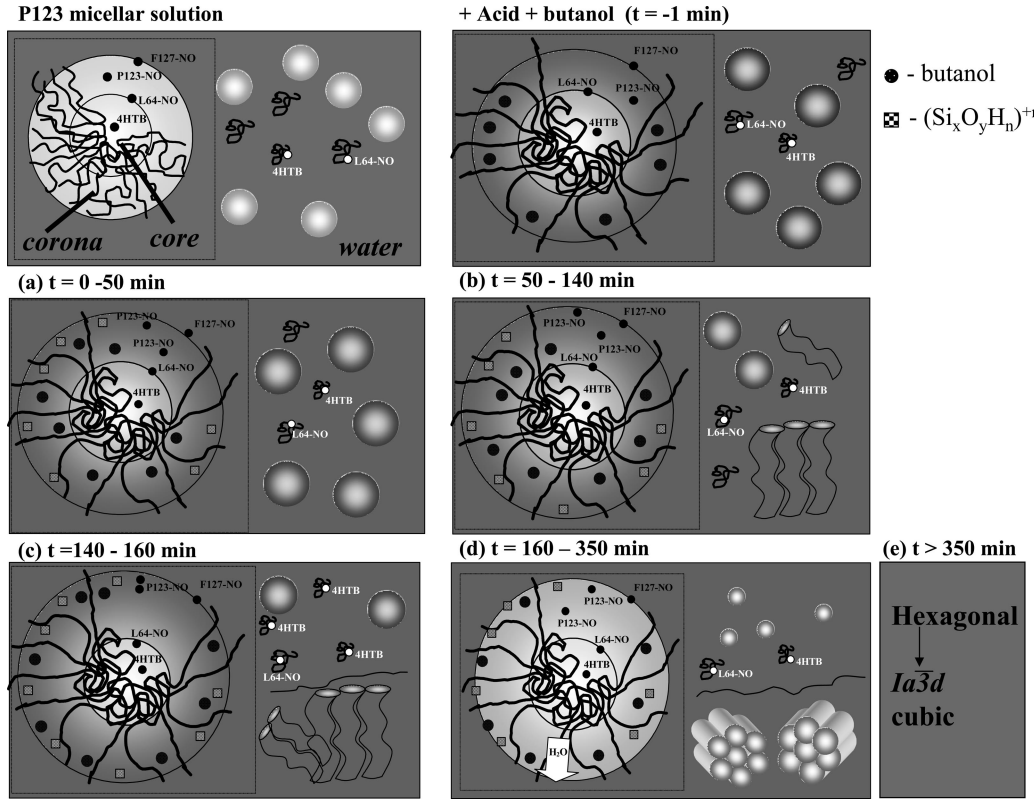

Figure 11. Proposed model for the five steps observed in the formation of KIT-6. The right-hand side of each panel presents the nanostructures present in the reaction mixture at a given time. The left side of each panel shows a cross section of the micellar structure with the location of the different probes within the micelles. Gray scale represent the amount of water in the corona region: dark gray denotes a large amount of water, whereas light gray denotes a region with less water.

probes dissolved in P123 single chains or small oligomers, because 4HTB is water insoluble. This is consistent with its τ_c value, which is larger than for 4HT in water but smaller than the corresponding τ_c (phob). The extent of the L64-NO and 4HTB in dissolved single chains is, however, small, 6% and 15%, respectively.

The addition of butanol to the P123 micellar solution induces penetration of butanol and water molecules into the corona (as indicated by an increase of $k(^2H)$ in the D_2O solution), expanding the micelle, without changing significantly R_{phob}, a_N, and τ_c.

To summarize, 4HTB probes the hydrophobic core of the micelles and single chains in the solution, L64-NO the core−corona interface and single chain, P123-NO the corona, and F127-NO the corona−water interface of the micelle. Figure 11 illustrates the location of the probes in the micellar solution.

Formation Mechanism. The EPR experiments resolved five clear stages: (a) 0–50 min, (b) 50–140 min, (c) 140–160, (d) 160–350 min, and (e) $t > 350$. At the precipitation time (∼150 min) there is a reorganization of the micellar structure accompanied by acceleration of the rate of condensation of the silica during the following stage (d). This is associated with a depletion of water and butanol from the core/corona regions. The cryo-TEM and FFR micrographs revealed the formation of TLMs prior to precipitation, coexisting with spherical micelles (stages (a) and (b)). At the end of (b), just before precipitation, aggregation of TLMs was observed and transformation to a hexagonal structure was detected during (d). In the following we discuss in more details the events of each stage, as sensed by the different spin-probes.

(a) 0–50 min. During this time condensation of the silica oligomers at the micelle/water interface takes place and reduces the mobility of F127-NO as manifested by the increase in τ_c. This process is associated with a considerable depletion of water and butanol molecules at the core−corona interface, as detected by ESEEM measurements of 4HTB and P123-NO. This depletion is most pronounced within the first 20–30 min.[53] During this time a second environment, "phil", has developed for P123-NO (its assignment will be discussed later). At this time only spherical micelles are present, showing that the curvature of the micelles has not yet reached the critical value needed to induce elongation of the spherical micelles.

(b) 50–140 min. During this stage only mild changes are observed at the molecular level, primarily a decrease of a_N(phob) of L64-NO and of R_{phob} of 4HTB and an increase of τ_c of F127-NO. This indicates that the silica condensation still takes place, but at a reduced rate, as observed by the mild reduction in $k(^2H)$ of 4HTB showing that water depletion still takes place. Nonetheless, at this time a

(52) This is different than L62-NO in the precursor P123 micelles of the SBA-15 synthesis where only a single environment, "phob", was observed and assigned to the corona.[5] There, the concentration of the P123 was slightly higher (3 wt %), and the temperature was higher (50 °C), further away from the monomer−micelle transition temperature, and therefore L62-NO in a single chain was not detected.

(53) These water molecules are remote molecules, because a_N measured by CW EPR was not sensitive to this depletion.

transition from spherical micelles to TLMs occurs, induced by the progressive dehydration of the Pluronics, which lowers the micelle curvature, reaching the necessary critical point for the transition. Moreover, toward the end of the period TLMs aggregate. It is interesting that this transition and aggregation occur some time after the larger molecular level changes are observed during stage (a).

(c) 140–160 min. The most sensitive probes of the precipitation (phase separation) are 4HTB and P123-NO. During this time there is some reorganization of the micellar structure which involves a momentary reduction of the size of the hydrophobic core, while increasing its hydrophobicity. This leads to a shift in the equilibrium toward dissolution of 4HTB in P123 single chains/small oligomers present in the dilute phase. During this time there is also a significant shift of P123-NO from "phob" to "phil", where the difference in their a_N and τ_c values becomes negligible (see Table 2). This suggests that as opposed to L64-NO and 4HTB, where the "phil" environment is single chains, the "phil" environment of P123-NO is at the corona/water interface. Concomitantly with the size decrease of the hydrophobic core there is an increase in the size of the corona associated with some effective stretching of the EO chains as manifested in the displacement of the P123-NO toward a more hydrophilic environment, the corona−water interface. As the precipitation proceeds, the amount of the concentrated phase increases and 4HTB molecules shift back to the micelle's core, the size of which has increased, although R_{phob} remains a little smaller than prior to precipitation (Table 2). Similarly, P123-NO goes back into the corona region, and the amount of its "phil" species decreases, although its a_N remains smaller. In addition, τ_c of its "phob" species is restored.

Just prior to precipitation the cryo-TEM micrograph shows aggregation of TLMs. Such aggregation would cause an effective increase of the corona, because the corona of several TLMs combines and water molecules are driven out due to the increase in van der Waals interaction between the Pluronics, decreasing the polarity as observed by P123-NO.

In contrast to 4HTB and P123-NO, L64-NO does not exhibit any abrupt changes during precipitation. The reduction of the size of the hydrophobic core displaces some probes into single chains or solution, rather than to the corona−water interface, as observed for P123-NO, probably due to its shorter chains. The decrease in R_{phob} is, however, small compared to 4HTB. The latter is a much smaller molecule and therefore can migrate easily from one environment to the next. Consequently, the displacement of L64-NO occurs at a slower rate than for 4HTB. Furthermore, R_{phob} is not restored to its original value as observed for P123-NO. This is consistent with a smaller displacement of the P123-NO that is limited to movement within the corona region, as compared to a single polymer chain penetrating the TLM aggregates.

(d) 160–350 min. During this time an accelerated silica condensation is detected by a higher rate of the increase of τ_c of F127-NO, along with an increase in the rate of the depletion of water and butanol molecules from the core/corona, detected by ESEEM of 4HTB and P123-NO. This depletion reduces the polarity of the corona, as manifested by the decrease in a_N of both L64-NO and P123-NO. This accelerated silica condensation is associated with the transformation from aggregated TLMs into a hexagonal structure.

(e) $t > 350$ *min.* From 350 min on, no more changes were observed at the molecular level by the EPR experiments, and after 24 h of reaction, the majority of the Pluronic spin-probes are dissolved in the corona and 4HTB in the core of the organic aggregates. However, after drying, some of L64-NO and P123-NO are found in the mesopores. This suggests that the drying process displaces P123 EO segments from the corona region, where the silica condenses, into the "core" which is the precursor of the mesopores. Because we have not observed the cubic structure in solution, we cannot exclude the possibility that the hexagonal−cubic transformation is induced by drying, although it is unlikely.

Figure 11 presents a schematic model that summarizes the five steps in the formation of KIT-6, prior to drying. In the left side of each panel, a cross-section of the micellar structure (spheroidal or TLM) with the location of the different probes within the micelles are shown. The right-hand side of each panel presents the nanostructures present in the reaction mixture at the given time.

Role of Butanol. Butanol is known to act as a cosolute in block copolymer−water systems, which co-micellizes with the block copolymer and stabilizes apolar–polar interfaces, determining the micellar interfacial curvature.[54,55] Butanol can interact with both PEO and PPO blocks, with its polar −OH headgroup assumed to be located mostly at the hydrophilic−hydrophobic interface of the micelles.[54,55] Prior to the addition of TEOS, the ESEEM experiments showed that butanol is preferably located in the corona region, and its penetration into the corona fills the micelles with water. Then during stage (a) there is movement of the butanol from the corona to the core−corona interface, and during stage (b), when TLMs form, no significant changes in its location were observed. At stage (d), when the formation of an hexagonal phase was observed, the butanol molecules were displaced into a more hydrophilic environment, namely, the corona−water interface. This displacement of the butanol may be responsible for further decrease in the interfacial curvature of the TLMs that compose the hexagonal structure, which induces the formation of the bicontinuous $Ia\bar{3}d$ cubic phase, which has a higher g value ($g > 1/2$) than the hexagonal phase.[13]

Kim et al.[13] showed that at a fixed amount of TEOS, increasing the amount of butanol results in a transition from a 2D hexagonal to $Ia\bar{3}d$ cubic mesophase, to, finally, a distorted phase. In addition, at fixed butanol and TEOS concentrations, an increase in the acid amount yields a transition from cubic to hexagonal phase. They summarized by noting that the cubic phase is formed at a certain low acid concentration and a certain range of butanol concentration. However, they did not report on changing the composition of the reaction mixture during the reaction. In an earlier study, Firouzi et al.[21] showed that a change of pH of reaction

(54) Holmqvist, P.; Alexandridis, P.; Lindman, B. *J. Phys. Chem. B* **1998**, *102*, 1149.
(55) Holmqvist, P.; Alexandridis, P.; Lindman, B. *Macromolecules* **1997**, *30*, 6788.

mixture of MCM-41 induces a transition from a lamellar silicatropic liquid crystal to a hexagonal one. This was possible only when the silica polymerization was inhibited by the addition of alcohol.

We showed that butanol added to a reaction mixture of SBA-15, after the formation of the hexagonal arrangement but when the silica is not yet fully polymerized, generates the $Ia\bar{3}d$ cubic phase. This emphasizes the significance of butanol in the phase transformation from hexagonal to cubic. In addition, this experiment showed that the amount of acid is not critical, and even at high acid concentration as in the SBA-15 synthesis, the cubic phase forms. The amount of acid, however, determines the rate of silica hydrolysis and condensation and the rate of formation of the hexagonal phase.[32]

The importance of additives to the formation of the $Ia\bar{3}d$ cubic phase was also studied by Flodström et al.[25,56] and Baute and Goldfarb.[57] They showed that an increase of salt concentration leads to an increase in the hydrophobicity of the corona of the P123 micelles, changing the curvature, and forming the $Ia\bar{3}d$ cubic phase. At low salt concentration a hexagonal phase was formed.

Comparison with Other in Situ Studies on Cubic Mesoporous Materials. Flodström and co-workers studied the formation of two different cubic systems.[25]The first was a cubic system based on a micelle structure ($Im\bar{3}m$), synthesized with Pluronic F108 ($EO_{132}PO_{50}EO_{132}$) and NaCl. The second is the bicontinuous cubic mesophase ($Ia\bar{3}d$), similar to KIT-6, but synthesized with Pluronic P103 ($EO_{17}PO_{59}EO_{17}$) and NaI. The methods they applied to study the formation of the cubic phase were in situ time-resolved small-angle synchrotron X-ray scattering, in situ time-resolved ^{1}H NMR, and time-resolved TEM. The TEM measurements were done on samples that were quenched by dilution at a particular time, followed by filtration and drying, as opposed to our cryo-TEM measurements, where portions of reaction mixture were virtified. The $Im\bar{3}m$ cubic phase was found to form via a transformation from unordered micelles directly to the micellar cubic structure after 1 h, without an intermediate structure. In the case of the bicontinuous system, the reaction occurred very fast, within minutes, and the authors believed that the system started from a disordered bicontinuous structure induced by the salt addition (micro-true liquid crystal mechanism) that transformed into an ordered one within minutes. The formation mechanism of these two cubic systems is very different from what we observed for KIT-6 by EPR and cryo-TEM. This suggests that different reaction conditions lead to different mechanisms. Moreover, it is possible that fast reaction of the bicontinuous cubic system with P103 and NaI prevented the detection of intermediate structures.

Kim et al.[13] investigated the formation mechanism of KIT-6 by stopping the reaction at different times, drying the solids, and measuring SAXS. Although the drying process may cause a change of phase, they claimed that the cubic phase is formed via a transformation from a lamellar phase, appearing after 4–6 h. This is consistent with our results that the formation of the cubic phase occurs through a formation of mesophase with a lower curvature, lamellar or hexagonal.

Pevzner and Regev[58] investigated the formation of the bicontinuous cubic MCM-48 by in situ SAXS. They found that it formed through several phase transformations. In the early stages of the reaction, hexagonal and lamellar phases coexisted, and the final cubic phase resulted from the collapse of a preceding hexagonal phase. This further supports the argument that the bicontinuous cubic phase is formed through an intermediate structure with a higher curvature.

Comparison with the Formation of Hexagonal SBA-15 Mesoporous Material. Recently, we reported a model for the formation of the hexagonal SBA-15 based on cryo-TEM and EPR measurements.[24,32] There, too, only spheroidal micelles were present in the initial reaction mixture. When silicate oligomers are formed within the corona of the micelle, dehydration takes place, and a decrease in the curvature of the corona region occurs, followed by the elongation of the micelles to form TLMs. These TLMs became less flexible and straighter with the progression of the condensation of silica oligomers. Then TLM bundles appear, and precipitation occurred. The hexagonal phase forms after precipitation. This structural evolution is similar to that of KIT-6, with the exception of the final transformation of the hexagonal phase to the cubic $Ia\bar{3}d$ phase.

The SBA-15 reaction was followed by in situ EPR and ESEEM using L62-NO ($EO_6PO_{30}EO_6$).[5] Initially, L62-NO was distributed only in one environment, the micelle corona, and then at the very early stages of the reaction, the spin-probe partitioned between two different environments within the micelles, the corona and the core. There, as opposed to L64-NO in KIT-6, the τ_c values of the species were similar and considerably larger than τ_c of just the spin-probe in water. The difference between the two components was only in the a_N values (Table 2). The formation of a solution L64-NO in the KIT-6 reaction may be due to the presence of butanol.

Three stages were identified in the SBA-15 reaction: before precipitation, after precipitation time up to the formation of the hexagonal structure, and after the formation of the hexagonal structure. In the first two stages the environment of the "core" species became more and more hydrophobic, due to depletion of water molecules from the core−corona interface. In addition, an increase in the core size was observed. This displacement of the spin-label into the core reduced the amount of "corona" species from 100% at t = 0 min to 50% at the end of the reaction (t = 20 h). After the hexagonal structure had formed, no more changes had been detected by EPR. The major difference between the reaction of SBA-15 and that of KIT-6 is that in the latter a reduction in the core size was observed at the precipitation time, whereas in SBA-15 an increase in the hydrophobic core was detected. This can be accounted for by the addition of butanol to the reaction which changed the hydrophilicity at the core−corona interface. In addition, the use of different acids, H_3PO_4 (SBA-15) and HCl (KIT-6), could also play a role. In both KIT-6 and SBA-15 the formation of TLMs, induced by the condensation of silica oligomers within the corona, is an essential stage.

(56) Flodström, K.; Alfredsson, V.; Källrot, N. *J. Am. Chem. Soc.* **2003**, *125*, 4402.
(57) Baute, D.; Goldfarb, D. *J. Phys. Chem. C* **2007**, *111*, 10931.

Conclusions

The formation mechanism of the cubic mesoporous material KIT-6 was investigated on both the molecular and the mesoscale levels. The addition of butanol to the initial micellar solution causes swelling and a surge of water molecules to the corona. Then, with the addition of TEOS, five main stages were resolved. (a) 0–50 min: only spheroidal micelles are present, and condensation of the silica oligomers takes place at the micellar/water interface and within the corona, causing a depletion of water and butanol molecules from the core-corona interface. This condensation lowers the mobility of the ends of the Pluronic chains located at the corona−water interface. (b) 50–140 min: the changes at the molecular level are mild, showing the continuation of water depletion, and TLMs appear. Toward the end of this period the TLMs aggregate. (c) Precipitation time (140–160 min): the core of the aggregated TLMs becomes more hydrophobic and reduced in size, while the size of the corona increases. (d) 160–350 min: the silica condensation is accelerated, leading to large depletion of water and butanol from the corona, and the core size increases, along with a decrease in the polarity of the core and corona regions. The aggregated TLMs transformed into a hexagonal structure. (e) 6−24 h: no changes are detected on the molecular level, and the transition from hexagonal to cubic phase occurs.

It was further shown that butanol is not essential in the earlier stages of the reaction, and can be added after the formation of the hexagonal phase (during stage (e)). The final material is characterized by ordered mesopores and micropores, where the extent of microporosity decreases remarkably after the hydrothermal treatment.

Acknowledgment. The authors thank Mr. Ilia Kaminker for help in preforming the SAXS measurements. Acknowledgment is given to the Donors of the American Chemical Society Petroleum Research Fund for partial support of this research. This research was supported by a grant from the Ministry of Science, Israel, awarded to S.R. D.G. holds the Erich Klieger Professorial chair in Chemical Physics. This research is made possible in part by the historic generosity of the Harold Perlman Family. The cryo-TEM work was carried out at the Harnnah and George Krumholz Laboratory for Advanced Microscopy, part of the Technion Project on Complex Fluids, Microstructure and Macromolecules, and supported by a grant from the Technion Russell Berrie Nanotechnology Institute (RBNI).

CM7025619

(58) Pevzner, S.; Regev, O. *Microporous Mesoporous Mater.* **2000**, *38*, 38.